AGU PUBLICATIONS

JGR

Journal of Geophysical Research: Atmospheres

RESEARCH ARTICLE
10.1002/2014JD022516

**Special Section:**
Fast Physics in Climate Models: Parameterization, Evaluation and Observation

**Key Points:**
- Field observational experiments
- Three typical underlying surface in northwestern China
- Land surface spectral radiation and albedo

**Correspondence to:**
Z. Wei,
wzg@bnu.edu.cn

**Citation:**
Zheng, Z., W. Dong, Z. Li, W. Zhao, S. Hu, X. Yan, J. Zhao, and Z. Wei (2015), Observational study of surface spectral radiation and corresponding albedo over Gobi, desert, and bare loess surfaces in northwestern China, *J. Geophys. Res. Atmos.*, *120*, doi:10.1002/2014JD022516.

Received 4 SEP 2014
Accepted 23 DEC 2014
Accepted article online 30 DEC 2014

# Observational study of surface spectral radiation and corresponding albedo over Gobi, desert, and bare loess surfaces in northwestern China

**Zhiyuan Zheng[1], Wenjie Dong[1], Zhenchao Li[2], Wei Zhao[1], Shanshan Hu[1], Xiaodong Yan[1], Jiaqi Zhao[3], and Zhigang Wei[1]**

[1]State Key Laboratory of Earth Surface Processes and Resource Ecology, Beijing Normal University, Beijing, China, [2]Key Laboratory of Land Surface Process and Climate Change in Cold and Arid Regions, Cold and Arid Regions Environmental and Engineering Research Institute, CAS, Lanzhou, China, [3]Songyuan Meteorological Bureau, Songyuan, China

**Abstract** In this paper, the field experiments on ground surface spectral broadband solar radiation (SR) and corresponding albedo were introduced at three man-made sites at Gobi, desert, and bare loess zones during three different intensive observational periods (IOP) from 2010 to 2013 in Gansu Province, respectively. The continuous and high temporal resolution records of ground surface solar radiation are presented, including global (GR), ultraviolet (UV), visible (VIS), and near-infrared radiation (NIR). The corresponding albedos are analyzed over three typical nonvegetated underlying surfaces in arid and semiarid and semihumid regions of northwestern China. The preliminary investigations were carried out. The results show that the variation trends of UV, VIS, and NIR are coincident with the GR, and the irradiances are gradually decreasing throughout the IOP at each site; the energy ratios of VIS/GR are all approximately 40.2%, and the ratios of NIR/GR are all approximately 54.4% at the Gobi, desert, and bare loess zones; and the averaged albedos of the soil for VIS are 0.231, 0.211, and 0.142 and for the NIR are 0.266, 0.252, and 0.255 over the Gobi, desert, and bare loess land surfaces, respectively. The energy ratios of VIS/GR and NIR/GR are not 50% as prescribed for all of the soil color classes in most of land surface models (LSMs). The observational soil albedo values for NIR are not twice to that of the VIS as predicted in some LSMs for the underlying surface at the three sites. GR albedo is determined by the energy ratios of SR/GR and SR albedos.

## 1. Introduction

The global climate has undergone significant changes over the past several decades [*Barnett et al.*, 1999; *Trenberth et al.*, 2007; *Cox and Stephenson*, 2007]. Although other features are recognized as equally important consequences of global climate change, changes in average air and ground temperatures have been the most apparent [*Jones et al.*, 1999; *Soloman et al.*, 2007; *Overpeck et al.*, 2011; *Stocker et al.*, 2013; *Ji et al.*, 2014; *Wang*, 2014], and global temperature has become the primary metric of global climate change [*Wang and Dickinson*, 2013]. The overall increase in global temperature over the last century is largely attributed to anthropogenic and natural and external factors, e.g., increases in greenhouse gas, aerosol and nitrogen oxides, and changes of cloudiness and cloud pattern in the upper troposphere, etc. [*Kiehl and Trenberth*, 1997; *Tett et al.*, 1999; *Barnett et al.*, 1999, 2005; *Trenberth et al.*, 2007; *Knutti and Hegerl*, 2008; *Mercado et al.*, 2009; *Murphy et al.*, 2009; *Trenberth and Fasullo*, 2009; *BurkHardt and Karcher*, 2011; *Huber and Knutti*, 2011; *Rigby et al.*, 2014].

Surface incident solar global radiation sustains life and shapes the structure of environment, weather, and climate patterns on Earth [*Trenberth et al.*, 2008]. It is the source of a variety of physical processes in the climate system and is one of the most important factors affecting the climate system and environment. It drives the interactions between the Earth's surface and atmosphere while also affecting surface substance and energy variations [*Wang et al.*, 2001, 2002a, 2002b, 2013]. It has been extensively studied by using various radiometers to examine whether the variations of surface incident solar radiation have partially caused observational decadal temperature variability trends [*Wang et al.*, 2013; *Wang and Dickinson*, 2013].

Land surface albedo is defined as the fraction of incident solar energy reflected by the land surface over the solar spectral domain [*Dickinson*, 1983, 1995; *Tsvetsinskaya et al.*, 2002; *Z. Wang et al.*, 2004; *N. F. Liu et al.*, 2013; *Q. Liu et al.*, 2013]. It directly controls the net solar radiation absorbed at the surface. Hence, it significantly affects surface energy and energy budget redistribution. As one of the fundamental forcing

parameters of general circulation models, hydrology models, numerical weather models, and climate models, surface albedo plays an important role in shaping the Earth's radiation energy budget and determining Earth surface temperature and evapotranspiration [*Dickinson*, 1995; *Manalo-Smith et al*., 1998; *Xue et al*., 1991; *Z. Wang et al*., 2004; *Barnes and Roy*, 2008, 2010; *Trenberth and Fasullo*, 2009; *Liang et al*., 2010; *Loew and Govaerts*, 2010; *Bala and Nag*, 2012; *Q. Liu et al*., 2013; *Qu et al*., 2013; *Meng et al*., 2013]. Spatiotemporal variability in surface albedo is often associated with environmental change and human activities [*Wilson et al*., 1987; *Dirmeyer and Shukla*, 1994; *Moritz et al*., 2002; *Jin and Roy*, 2005; *Bsaibes et al*., 2009; *N. F. Liu et al*., 2013]. One of the most important feedback processes in the climate system related to land ground surface and atmosphere is the land-albedo feedback. It results from the ability of the ground surface to reflect solar radiation back to the atmosphere and the relationship between this ability and temperature. Surface albedo decreases with the warming in ground and air temperature, and then can lead to further warming. Consequently, more irradiance reaches the ground, more energy imbalance turns out. This is the famous biogeophysical feedback mechanism driven by albedo that was first proposed by *Charney* [1975], who proved that human activity increases stress on vegetation cover. The stress may in turn further increase surface albedo, thus facilitate the occurrence of drought. Hence, a positive feedback mechanism with rainfall may then further increase albedo [*Charney et al*., 1977; *Dickinson and Hanson*, 1984]. The land-albedo feedback mechanism has been studied extensively through incident and reflected irradiance measurements and surface physical properties. *Courel et al*. [1984] pointed out the persistence of Sahel drought between 1973 and 1979 can be attributed to Charney's land-albedo feedback mechanism. Hence, global albedo effect is very pivotal to understanding the mechanisms of climate change [*Wielicki et al*., 2005; *Loew and Govaerts*, 2010; *Liang et al*., 2013; *Q. Liu et al*., 2013; *N. F. Liu et al*., 2013].

Space-borne remote sensing has major advances in study of climate system and climate change, by providing valuable information on the state of the Earth-atmosphere system and its components, and by quantifying atmospheric processes and spatial-temporal states of the atmosphere, land and oceans in an area-wide and continuous way. Over the past few decades, comprehensive satellite platforms with numerous sensors have been constructed to monitor a wide range of atmospheric parameters examined in meteorological and climatological studies, and the information retrieved from these satellite-based sensors has greatly enhanced our understandings of processes and dynamics within the Earth-atmosphere system [*Wielicki et al*., 2005; *Liang et al*., 2010; *Thies and Bendix*, 2011; *Yang et al*., 2013]. Albedo has been shown to be impacted by complex combinations of soil classes and solar elevation angle. Land surface albedo can now be obtained via satellite remote sensing [*Xue and Cracknell*, 1995; *Wielicki et al*., 2005; *Bsaibes et al*., 2009; *Loew and Govaerts*, 2010; *Liang et al*., 2010, 2013; *Q. Liu et al*., 2013; *N. F. Liu et al*., 2013]. Spectral albedo measurements give rise to more detailed analyses of ground surface properties.

However, satellite remote sensing also has a number of its own limitations. Analyzing albedo spectrums can be used to describe different processes without carrying out extra in situ measurements as long as the processes have been known that they have a known effect on spectral albedo. Furthermore, more spectral albedo data sets are needed to validate and calibrate optical and microwave remote sensing instruments. Time series data sets on spectral albedo are sparse because it is difficult to measure spectral radiation accurately at high levels of temporal resolution on the technical and theoretical level [*Wei et al*., 2001; *Nikitidou and Kazantzidis*, 2013; *Wang et al*., 2013].

Routine irradiance measurements are very valuable to climate change research due to their long time series and broadband wavelength coverage. Ground surface solar radiation and corresponding albedo in arid and semiarid and semihumid regions significantly can affect local and global energy balances and hydrothermal circulation, and then they have been received considerable worldwide attention [*Charney*, 1975; *Charney et al*., 1977; *Courel et al*., 1984; *Dickinson and Hanson*, 1984]. The majority of ground surface radiation measurements have been limited to spot measurement and in situ measurement of four-component net radiation in China [*Zhang and Zhou*, 2002; *Ji et al*., 2003, 2004; *Yang et al*., 2005; *Wang et al*., 2005, 2012; *Wei et al*., 2005; *Chen et al*., 2006; *Li et al*., 2008, 2009; *Ding et al*., 2013; *Ao et al*., 2013]. Few studies have analyzed surface spectral broadband solar radiation (hereinafter, referred to as SR) and corresponding albedo in China [*Wei and Lin*, 1992; *Ji et al*., 1993; *Jiang*, 1993; *Xiong et al*., 1994; *Zhang et al*., 1996; *Bai et al*., 1998; *Zheng et al*., 2012]. As well, relatively little is known of surface ground SR features, the ratios of SR to ground surface global radiation (hereinafter, referred to as GR) and their accurate values of soil albedo for ultraviolet radiation (hereinafter, referred to as UV), visible radiation (hereinafter, referred to as VIS) and near-infrared radiation (hereinafter, referred to as NIR) in northwestern China. Quantifying these parameters is very critical

to understanding land-atmosphere interactions, verifying, improving, and developing land surface models (hereinafter, referred to as LSMs), and making sure how these factors may alter future weather and climate patterns in northwestern China. Despite the importance of such data sets, high-resolution time series measurements of these properties are not widely available, primarily because such observations involve first overcoming several technical and logistical challenges, such as ensuring that sensors remain clean and level [*Nicolaus et al*., 2010].

This paper presents a limited exploratory study which try to investigate whether the energy ratios of SR/GR and spectral albedo values assigned in LSMs are correct for arid and semiarid and semihumid regions in northwestern China. Consequently, three-field observational experiments were conducted at three typical nonvegetated underlying surfaces during three different intensive observation periods (hereinafter, referred to as IOP) from 2010 to 2013. Ground surface GR and SR data sets were collected and used to analyze surface solar radiation and corresponding albedo characteristics in these areas. The present study quantifies the energy ratio of SR/GR and the values of soil albedo for UV, VIS, and NIR using the data sets all collected during IOP.

## 2. Review Soil Albedo Parameterization Scheme in LSMs

The identical or similar bare soil ground surface albedo parameterization schemes have been assigned in some main LSMs, e.g., Community Land Model (CLM) [*Oleson et al*., 2010, 2013], Common Land Model [*Dai et al*., 2003], Biosphere-Atmosphere Transfer Scheme [*Dickinson et al*., 1993], National Center for Atmospheric Research Land Surface Model [*Bonan*, 1996], Simple Biosphere Model [*Sellers et al*., 1986], and Simplified Simple Biosphere Scheme [*Xue et al*., 1991, 1996]. For most of LSMs, bare soil ground surface albedo varies with the soil color classes and soil moisture, and the community parameterization formula is

$$\alpha^{\mu}_{\mathrm{soi},\wedge} = \alpha_{\mathrm{soi},\wedge} = \left(\alpha_{\mathrm{sat},\wedge} + \Delta\right) \leq \alpha_{\mathrm{soi,dry}} \tag{1}$$

where $\alpha^{\mu}_{\mathrm{soi},\wedge}$ is the soil albedo for the direct beam, $\alpha_{\mathrm{soi},\wedge}$ is the soil albedo for the diffuse beam, $\theta$ is the volumetric water content of the first soil layer, $\alpha_{\mathrm{sat},\wedge}$ and $\alpha_{\mathrm{soi,dry}}$ are the albedos for saturated and dry soil color classes, and $\Delta = 0.11 - 0.40\theta > 0$ depends on $\theta$, respectively.

Bare soil albedo is a function of prescribed soil color type and surface soil moisture but independent of solar elevation angle. The lighter the color is, the higher the soil albedo is. Surface incident solar radiation is divided into the following four portions: direct and diffuse beams for visible ($\lambda < 700$ nm) and near-infrared ($\lambda > 700$ nm) wave bands, respectively. Bare soil albedo for the direct beam ($\alpha^{\mu}_{\mathrm{soil},\wedge}$) and for the diffuse albedo ($\alpha_{\mathrm{soil},\wedge}$) are prescribed as equally for each soil color class. The soil albedo for wave band of NIR is assumed to be twice those for VIS. A description of these features can be found in LSMs technical note [*Dickinson et al*., 1993; *Bonan*, 1996; *Dai et al*., 2003; *Oleson et al*., 2010, 2013].

In the CLM, dry and saturated soil albedos are determined by soil color [*Oleson et al*., 2010, 2013]. Soil thermal and hydrologic properties are determined by silt, sand, clay, and organic matter content. CLM soil colors are prescribed based on the results in the previous scientific study of *Lawrence and Chase* [2007]. The International Geosphere-Biosphere Programme soil data sets of 4931 soil mapping units and corresponding sand and clay contents for each soil layer are used to create mineral soil texture [*Bonan et al*., 2002] and organic matter density data sets [*Lawrence and Slater*, 2008] that vary with soil depth. These data sets can best represent the Moderate Resolution Imaging Spectroradiometer (MODIS) local noon surface albedo for each CLM grid cell. Soil colors are fitted for 20 soil types and are compared to the MODIS monthly local noon all-sky surface albedos [*Oleson et al*., 2010, 2013].

Based on the technical note and procedure of CLM, when the first soil layer volumetric water content $\theta_1$ is greater than or equal 0.257 $m^3\,m^{-3}$, the model will use the saturated soil albedo for the VIS to calculate ground surface albedo. Most of prevailing LSMs, the soil reflectance is assumed to be isotropic for all solar angles. A saturated soil albedo value is also assigned to each color class, and this assigns the soil albedo value for the NIR to be twice that of the VIS. The energy ratios of VIS/GR and NIR/GR are 50% as prescribed for all different soil color class in LSMs, respectively [*Dickinson et al*., 1993; *Bonan*, 1996; *Oleson et al*., 2010, 2013].

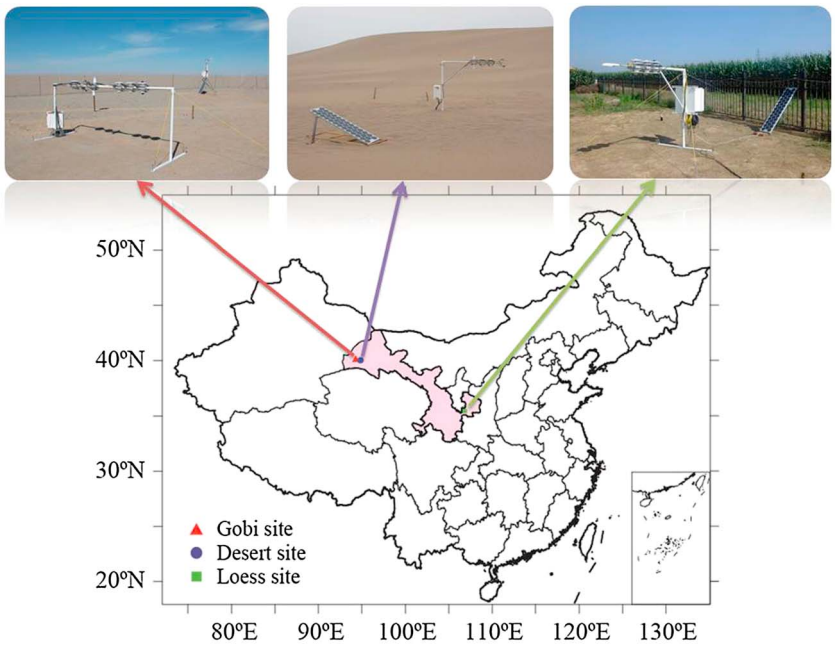


**Figure 1.** Spatial distribution of the three observational sites.

## 3. Materials and Methods

Field experiments were conducted at Gobi, desert, and loess sites during IOP, respectively. These sites were located in arid and semiarid and semihumid regions of Gansu Province in northwestern China, which were designed for quantifying the land-atmosphere interactions at typical nonvegetated bare soil underlying surfaces. They are representative of typical geomorphic feature of large areas in northwestern China. Figure 1 shows the spatial distribution of the three observational sites. Detail introductions of the three sites can be seen in section 3.1. Over the course of field experiments, the sensors were checked and cleaned daily to prevent water droplets, dust, and other materials from adhering to radiometer sensor domes.

### 3.1. Brief Description of Field Experiment Sites

#### 3.1.1. Gobi Site

The Gobi site was located at 40°10′N, 94°31′E at an altitude of 1150 m to the west of Dunhuang City, Gansu Province. The IOP was from 22 September to 21 October 2010. The site surrounding environment is typical characterized by bare, flat, and homogeneous Gobi. It can well represent the large Gobi area. The Gobi site ground surface is predominantly composed of small stones at the upper surface and fine sand at the lower surface. Climate type of this site belongs to the continental drought climate temperature zone where daily air temperature amplitude is very high. The maximum surface air temperature is 317 K, and the minimum temperature is 245 K. The annual average air temperature and precipitation in the region are 279 K and 39 mm, respectively, with 178 frost-free days per year over approximately the last 50 years [*S. Wang et al.*, 2004; *Wei et al.*, 2006].

#### 3.1.2. Desert Site

The desert site was located at 40°05′N, 94°40′E at an altitude of 1180 m to the south of Dunhuang City, Gansu Province. The IOP was from 8 July to 13 October 2013. The desert site was surrounded by small sand hills. The ground surface of desert site is covered by bare, flat, and homogeneous sand. Climate type and other environmental conditions at the desert site are similar to those of at the Gobi site. Extreme drought, low precipitation and high evaporation, high air temperature amplitudes are the predominant features of the desert site.

#### 3.1.3. Loess Site

The field experiment at loess site was carried out in the typical rain fed agricultural region of the Loess Plateau. The landscape of the Loess Plateau is topographically complex with many ridges, hills, ditches, and ravines [*Zhang et al.*, 2014]. The loess site was located at 35°35′N, 106°42′E at an altitude of 1592 m in

**Table 1.** Specifications of Measurement Instruments Technical Parameters Used at the Gobi and Desert Sites

| Feature | Global | Ultraviolet | Visible |
|---|---|---|---|
| Senor type | PSP | TUVR | SKE510 |
| Manufacturer | Eppley, USA | Eppley, USA | Eppley, USA |
| Sensitivity | 9 μV/W m$^{-2}$ | 150 μV/W m$^{-2}$ | 1 mV/100 W m$^{-2}$ |
| Spectral range | 280–2800 nm | 285–395 nm | 400–700 nm |
| Long-term stability | ±2% | ±2% | ±2% |
| Response time | 1 s | 5 ms | 10 ns |
| Linearity error | ±0.5% | ±2% | <0.2% |
| Cosine error | ±1% ($0° < Z < 70°$) ± 3% ($70° < Z < 80°$) | <±3.5% ($0° < Z < 70°$) ± 10% ($70° < Z < 80°$) | 3% |
| Temperature response | ±1%/°C (−20°C to +40°C) | ±0.3%/°C (−40°C to +40°C) | ±0.1%/°C (−35°C to +70°C) |

Pingliang City, Gansu Province. The IOP was from 25 July to 23 August 2013. Maize was planted around the site throughout the IOP. We installed our measurement instruments in an open-field area surrounded by maize. The ground surface is bare, flat, and homogeneous bare soil. Soil found in loess site was predominantly medium loam with a high proportion of silt. The soil is composed of 78% silt, 4% clay, and 18% sand at the upper 40 cm layer [*Zhang et al.*, 2009]. The site was located in a semiarid and semihumid climate zone. The maximum air temperature is 307 K, and the minimum air temperature was 249 K. The annual average air temperature and precipitation are 279 K and 510 mm, respectively, with 2425 h of sunshine and 170 frost-free days per year over approximately the last 60 years [*Wei et al.*, 2005].

### 3.2. Field Experiments

Field experiments were conducted at the three different sites during the IOP. The downward and upward GR irradiance (280–2800 nm), UV irradiance (280–400 nm), VIS irradiance (400–700 nm), NIR irradiance (700–2800 nm), four-component net radiation irradiance on a horizontal plane, and soil temperatures at different depths were measured, respectively.

The sets of spectral radiometers, manufactured by the Eppley Laboratory in USA, were used at the Gobi and desert sites. The other set of spectral radiometers, manufactured by the YH83/PH-FSP in China, were used at the loess site. GR, UV, and NIR irradiance were measured by using Precision Spectral Pyranometer (PSP), Total Ultraviolet Radiometer (TUVR), and SKE510 model radiometers at the Gobi and desert sites. GR, VIS&NIR, and NIR irradiance were measured by using WB280, JB400, and HB700 model spectral radiometers at the loess site. Weather conditions at the Gobi and desert sites are virtually sunny during the IOP. A few rainy days were being at the loess site. GR and SR were measured by using radiometers mounted at a height of approximately 1.5 m above the ground surface. The observation data were all sampled at 1 min intervals and averaged at 30 min intervals. All of the data were recorded by using a Data taker fitted with a Personal Computer Memory Card International Association memory card. Detailed measurement instrument technical parameters specification can be seen in Tables 1 and 2.

According to the measurement instruments used in this work (Tables 1 and 2), we do not have the all spectral radiation radiometers (UV, VIS, and NIR) at each site. The NIR irradiance was not measured directly at the Gobi and desert sites. The UV and VIS irradiance were not measured directly at the loess site. As the method

**Table 2.** Specifications of Measurement Instruments Technical Parameters Used at the Loess Site

| Feature | Global | Visible and Near Infrared | Near Infrared |
|---|---|---|---|
| Senor type | WB280 | JB400 | HB700 |
| Manufacturer | China | China | China |
| Sensitivity | 12.65 μV/W m$^{-2}$ | 11.20 μV/W m$^{-2}$ | 12.46 μV/W m$^{-2}$ |
| Spectral range | 280–2800 nm | 400–700 nm | 700–2800 nm |
| Long-term stability | ±2% | ±2% | ±2% |
| Response time | 1 s | 10 ms | 2 s |
| Linearity error | ±0.5% | ±2% | ±1% |
| Cosine error | ±1% ($0° < Z < 70°$) ± 2% ($70° < Z < 80°$) | <±3% | ±3% |
| Temperature response | ±0.5%/°C (−30°C to +70°C) | ±0.2%/°C (−40°C to +70°C) | ±0.1%/°C (−40°C to +70°C) |

used in the previous study [*Escobedo et al*., 2011], the missing one can be indirectly estimated by calculation using the other measurement values. The NIR irradiance at the Gobi and desert sites used in this work was indirectly estimated: NIR = GR − UV − VIS. The UV irradiance at the loess site used in this work was indirectly estimated: UV = GR − VIS&NIR. The VIS irradiance used in this work was indirectly estimated: VIS = VIS&NIR − NIR.

Standard micrometeorological measurements were also conducted at the Gobi and loess sites during the IOP, including measurements of four-component net radiation, wind speed, wind direction, air pressure, precipitation, air temperature, air relative humidity, soil temperature, and soil moisture at different depths. Because we only focus on surface SR and corresponding albedos in this paper, we do not conduct a detailed analysis of the micrometeorological data sets. All the measurement instruments used in this work have been calibrated at the beginning and end of the field experiments.

### 3.3. Data Quality Control

*Shi et al*. [2008] pointed out the effect of Earth's orbital changes on the amount of solar irradiance reaching the Earth surface can be ignored when the research temporal scale is a short-term time scales of less than 1000 year. The solar irradiance at the top of the atmosphere (hereinafter, referred to as TOA) is determined by latitude, day of year, and the solar constant. The daily solar irradiation $G_0$ at the TOA over a ground station can be calculated by the following formula [*Iqbal*, 1983]:

$$G_0 = 24\times\left({}^{3600}/_{\pi}\right)E_{sc}(1+\rho)\cos\varphi\cos\delta\times \\ \times\left[\left({}^{\pi}/_{180}\right)\omega_0 - \tan\omega_0\right] \tag{2}$$

where $E_{sc}$ is the solar constant, $\varphi$ is the latitude of the station, $\delta$ is the solar declination, $\omega_0$ is the sunset (sunrise) hour angle, and $\rho$ is the relative eccentricity correction; $\rho$, $\delta$, and $\omega_0$ are functions of day of year (hereinafter, referred to as DOY). The solar constrain is set as 1367 W m$^{-2}$.

Solar radiation at the Earth surface is also affected by atmospheric absorbing gases (mainly oxygen, water vapor, and ozone), cloud, and aerosols. Quality control (hereinafter, referred to as QC) for the upper limit for GR is mainly based on that GR should be smaller than extraterrestrial solar radiation $G_0$ (equation (2)) at the same geographical location. A strict lower limit for GR is actually difficult set. Even if the direct daily irradiation at the surface could tend to nil under heavy overcast conditions, the diffuse daily irradiation hardly ever reaches zero completely. No matter what the weather and environment are like, the surface always can receive some solar radiation during the day. It is obvious that a lower limit for GR larger zero is reasonable. The lower limit here is set as 3% of the incoming TOA solar irradiation, according to the scientific research of *Geiger et al*. [2002].

QC for GR and SR irradiance is mainly following the five principles:

1. Observed GR and SR irradiances should be lower than that at the top of atmosphere and greater than the lower limit at the same geographical location.
2. Upward irradiance should be lower than downward irradiance.
3. The energy ratio of UV/GR should be in the range of 2% to 10%. The ratio of VIS/GR should be in the range of 30% to 50%. The ratio of NIR/GR should be in the range of 40% to 60%. Otherwise, it is considered as questionable observation.
4. SR irradiances should be smaller than GR at each measurement time.
5. For each measurement time, UV should be lower than GR, VIS, and NIR, VIS should be lower than GR and NIR, NIR be lower than GR, and GR should be greater than or equal to the sum of SR, respectively.

### 3.4. Theoretical Surface Albedo Considerations

According to the definition of albedo, ground surface albedo can be calculated using the following formula:

$$\alpha_g = S_{up}/S_{down} \tag{3}$$

where $\alpha_g$ is the ground surface albedo, $S_{down}$ is the total downward short-wave radiation (solar radiation reaching the ground surface), and $S_{up}$ is the total upward short-wave radiation (solar radiation reflected by the ground surface), respectively. For this calculation, 30 min averaged data sets were used.

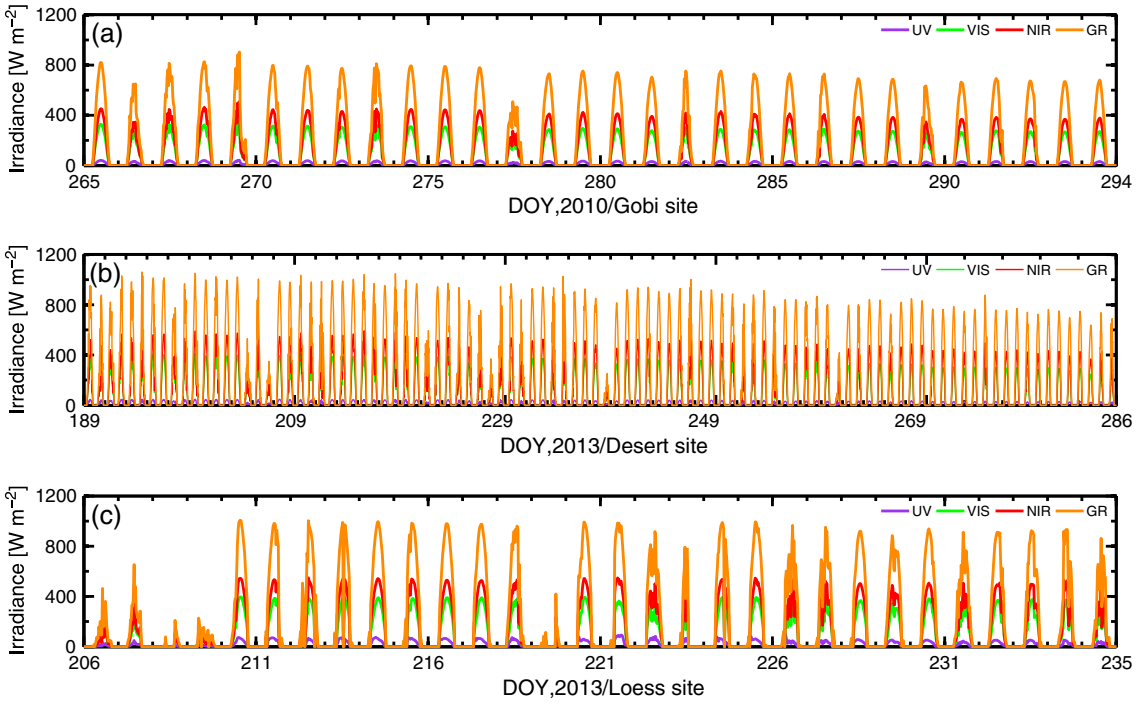


**Figure 2.** Variations of the SR and GR irradiance during the IOP at (a) the Gobi site, (b) the desert site, and (c) the loess site.

The daily averaged albedo is calculated according to the weight factor. According to methods in previous study *Wang et al.* [2008], the weighted averaged surface albedo can be calculated using the following formula:

$$\overline{\alpha}_g = \sum_{i=1}^{n} \frac{S_{\mathrm{down},i}}{\sum_{i=1}^{n} S_{\mathrm{down},i}} \alpha_{g_i} \tag{4}$$

where $\overline{\alpha}_g$ is the averaged ground surface albedo, $S_{\mathrm{down},i}$ is the total upward short-wave radiation for each measurement time, $\alpha_{gi}$ is the actual surface albedo for each measurement time, and $i$ is the measurement time, respectively. For this calculation, 30 min averaged data sets were used.

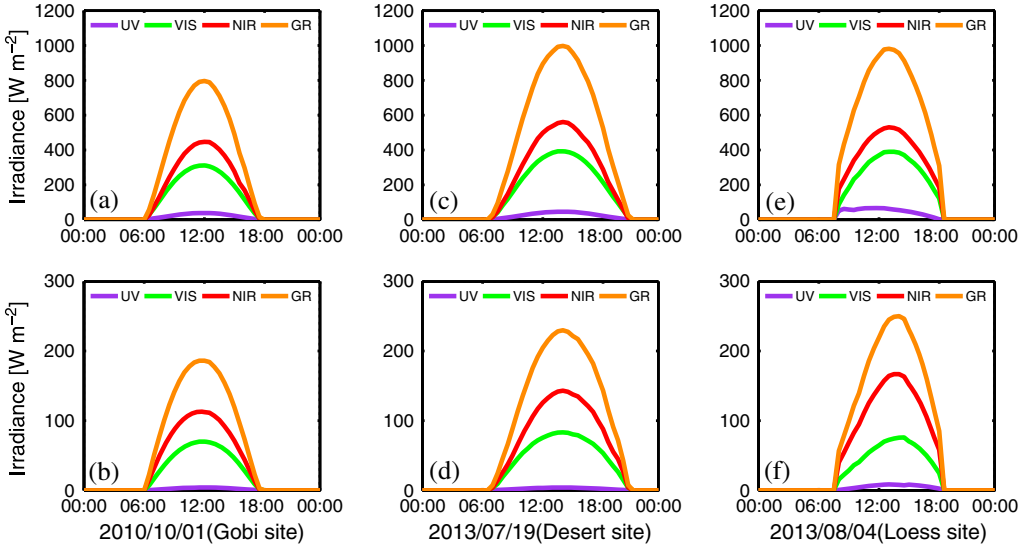


**Figure 3.** Diurnal cycles of ground surface radiation in typical sunny days during the IOP at the (a, b) Gobi site, (c, d) the desert site, and (e, f) the loess site, downward (Figures 3a, 3c, and 3e) and upward (Figures 3b, 3d, and 3f).

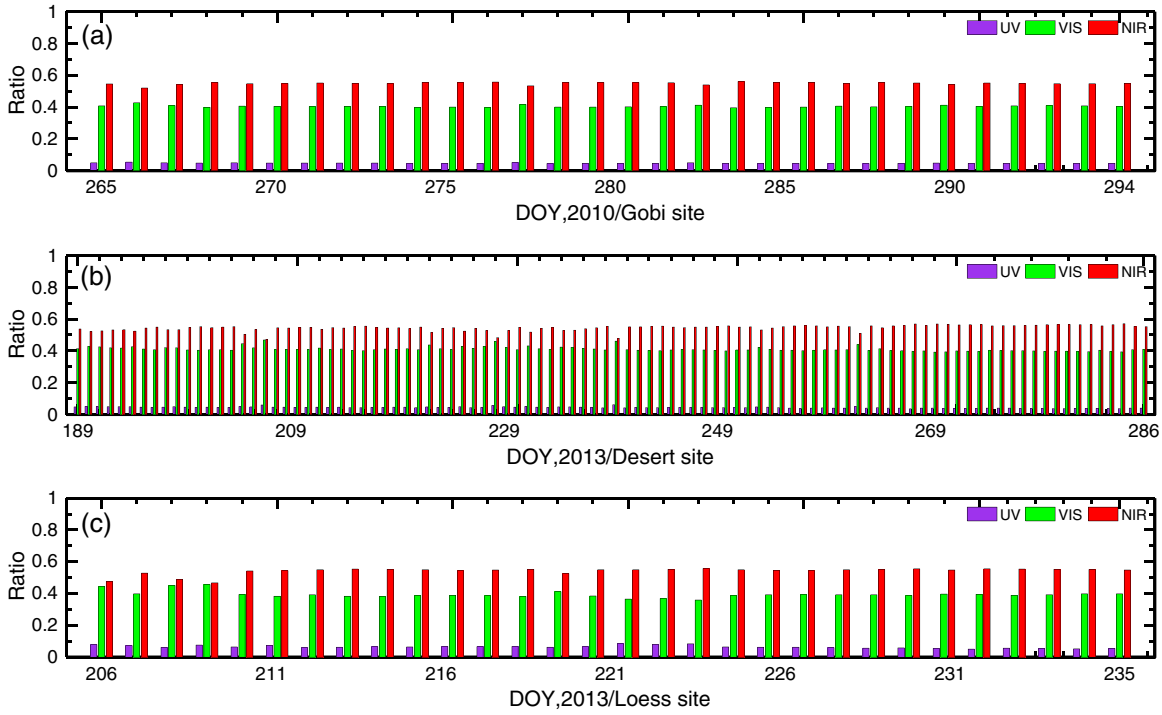


**Figure 4.** Variations of the averaged energy ratios of SR/GR during the IOP at (a) the Gobi site, (b) the desert site, and (c) the loess site.

## 4. Results

### 4.1. Radiation Components

Figure 2 shows temporal evolution of daily SR and GR irradiances during the IOP at the three sites, respectively. The variations of SR and GR show the same gradually decreasing trend over the entire observational period due to the seasonal transition and southward movement of the Sun. Overall UV, VIS, NIR, and GR irradiances were significantly affected by the synoptic conditions. Figure 3 shows the diurnal cycles of SR and GR in three typical sunny days at each site. The diurnal cycles of short-wave radiation obviously show a virtually identical regular trend and exhibit a symmetrical distribution shape. The maximum irradiance appeared at local noon. However, on cloudy day, the radiation cycles show an irregular trend and an asymmetrical distribution shape.

The variations of the averaged energy ratios of SR/GR are plotted in Figure 4. As shown in Figure 4, the energy ratios of SR/GR are almost constant at the three sites during the IOP. Statistical quantities of daily averaged energy ratios at each site are summarized in Table 3. The energy ratio of UV/GR was in the range of 3.5% to 8.5%, the ratio of VIS/GR was in the range of 36% to 46.8%, and the ratio of NIR/GR was in the range of 45.5% to 57.0%. The averaged energy ratios of VIS/GR and NIR/GR at three sites were approximately 40.2% and 54.4%, respectively. The result reveals that energy ratios of VIS/GR and NIR/GR do not account for 50% as prescribed in some LSMs [*Sellers et al*., 1986; *Xue et al*., 1991, 1996; *Dickinson et al*., 1993; *Bonan*, 1996; *Dai et al*., 2003; *Oleson et al*., 2010, 2013]. The VIS portion is lower than 50%, but the NIR portion is higher than 50%. The NIR portion is approximately 10%–15% higher than the VIS portion. That implies it is maybe necessary to

**Table 3.** Statistics on the Averaged Energy Ratios of SR/GR at Each Site (Unit: %)

| | Gobi Site | | | Desert Site | | | Loess Site | | |
|---|---|---|---|---|---|---|---|---|---|
| | Minimum | Maximum | Mean | Minimum | Maximum | Mean | Minimum | Maximum | Mean |
| UV | 4.5 | 5.4 | 4.7 | 3.5 | 6.1 | 4.4 | 5.0 | 8.5 | 6.5 |
| VIS | 39.4 | 42.7 | 40.4 | 39.2 | 46.8 | 41.1 | 36.0 | 45.0 | 39.4 |
| NIR | 51.9 | 56.0 | 54.9 | 47.4 | 57.0 | 54.6 | 45.5 | 55.6 | 53.8 |

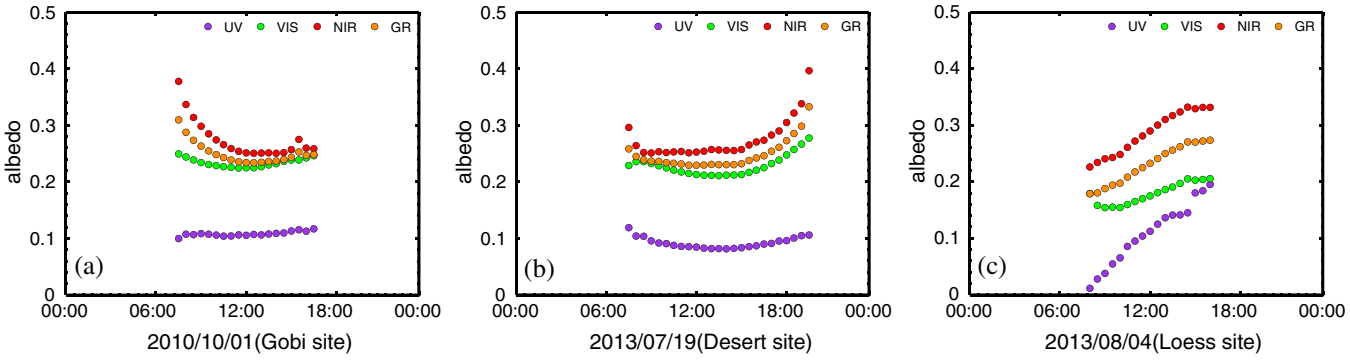


**Figure 5.** Diurnal cycles of SR and GR albedos in typical sunny days during the IOP at (a) the Gobi site, (b) the desert site, and (c) the loess site.

consider reinvestigating energy ratio allocation scheme in LSMs. If possible, we need to modify the default energy ratio values of VIS/GR and NIR/GR prescribed in LSMs.

### 4.2. Albedo Components

The diurnal cycles of ground surface albedo are shown in Figure 5 in three typical sunny days at the three sites, including SR and GR. In the typical sunny days at the Gobi and desert sites (Figures 5a and 5b), the diurnal cycles of surface albedos show a U type approximately. At the loess site, because it had been raining before 4 August 2013, the ground surface layer was very wet. The surface layer soil moisture now becomes the most important dominant factor affecting the bare soil surface albedo. As we all know, the bare soil albedo will decrease (increase) with the increase (decrease) of soil moisture. So the diurnal cycles of SR and GR albedos of sunny day diurnal cycles do not show a typical U type. The diurnal variations of surface albedos showed increasing lines on 4 August 2013 at the loess site, as shown in Figure 5c. The diurnal-averaged surface albedos were 0.258, 0.253, and 0.239 for GR, 0.109, 0.094, and 0.189 for UV, 0.234, 0.223, and 0.184 for VIS, and 0.292, 0.289, and 0.293 for NIR at the Gobi, desert, and loess sites, respectively.

Figure 6 shows the variations of the surface daily averaged albedos. Statistically, the daily averaged albedos for each site are summarized in Table 4. During the IOP, at the Gobi site, the daily averaged surface albedo

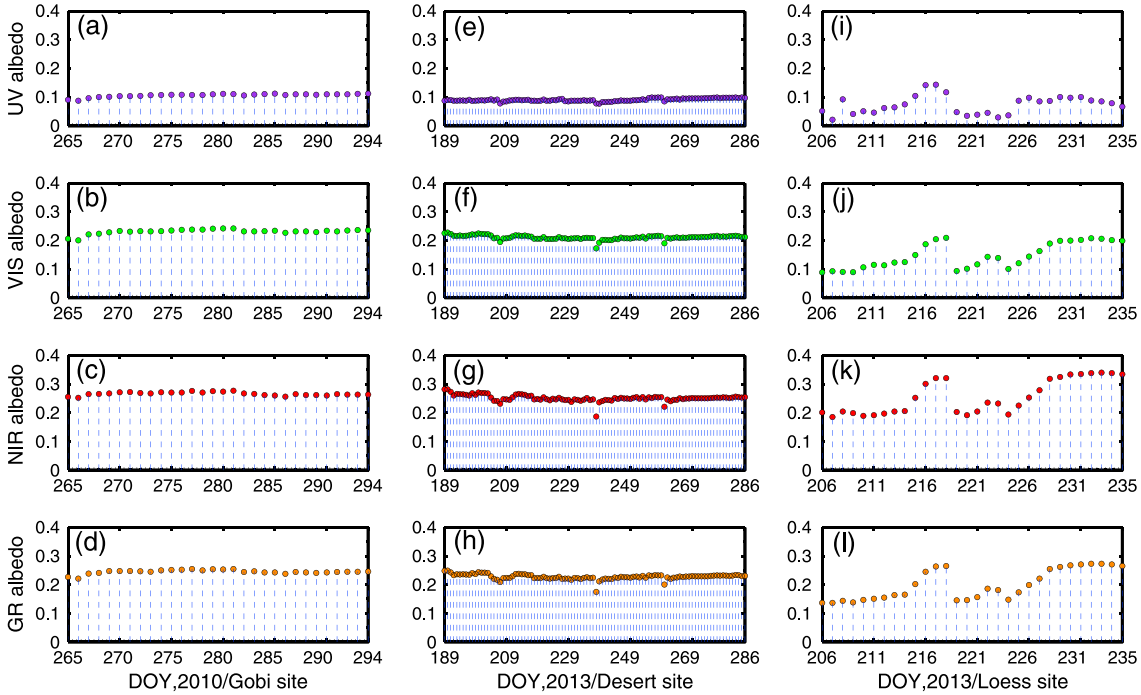


**Figure 6.** Variations of the averaged albedos during the IOP at (a–d) the Gobi site, (e–h) the desert site, and (i–l) the loess site.

**Table 4.** Statistics on the Averaged Albedos at Each Site

| | Gobi Site | | | Desert Site | | | Loess Site | | |
|---|---|---|---|---|---|---|---|---|---|
| | Minimum | Maximum | Mean | Minimum | Maximum | Mean | Minimum | Maximum | Mean |
| GR | 0.221 | 0.255 | 0.245 | 0.175 | 0.249 | 0.228 | 0.136 | 0.273 | 0.197 |
| UV | 0.088 | 0.112 | 0.107 | 0.078 | 0.099 | 0.091 | 0.021 | 0.144 | 0.074 |
| VIS | 0.20 | 0.242 | 0.231 | 0.172 | 0.228 | 0.211 | 0.059 | 0.208 | 0.142 |
| NIR | 0.252 | 0.277 | 0.266 | 0.187 | 0.282 | 0.252 | 0.186 | 0.340 | 0.255 |

wasin the range of 0.221–0.255 with an average value of 0.245 for GR (Figure 6d), in the range of 0.088–0.112 with an average value of 0.107 for UV (Figure 6a), in the range of 0.20–0.242 with an average value of 0.231 for VIS (Figure 6b), and in the range of 0.252–0.277 with an average value of 0.266 for NIR (Figure 6c). At the desert site, the daily averaged albedo was in the range of 0.175–0.249 with an average value of 0.228 for GR (Figure 6h), in the range of 0.078–0.099 with an average value of 0.091 for UV (Figure 6e), in the range of 0.172–0.228 with an average value of 0.211 for VIS (Figure 6f), and in the range of 0.187–0.282 with an average value of 0.252 for NIR (Figure 6g). At the loess site, daily averaged albedo was in the range of 0.136–0.273 with an average value of 0.197 for GR (Figure 6l), in the range of 0.021–0.144 with an average value of 0.074 for UV (Figure 6i), in the range of 0.059–0.208 with an average value of 0.142 for VIS (Figure 6j), and in the range of 0.186–0.340 with an average value of 0.255 for NIR (Figure 6k). As noted in section 3.2, there were many rainy days at the loess site during the IOP, so the bare soil surface albedos showed a different variation trend at loess site compared with at Gobi and desert site.

In summary, the daily averaged surface albedos are 0.231, 0.211, and 0.142 for VIS and 0.266, 0.252, and 0.255 for NIR at the Gobi, desert, and loess sites, respectively. These results indicate that the actual observational value of the bare soil albedo for NIR is not twice that of the VIS as prescribed for bare soil underlying surfaces in most LSMs [*Sellers et al*., 1986; *Xue et al*., 1991, 1996; *Dickinson et al*., 1993; *Bonan*, 1996; *Dai et al*., 2003; *Oleson et al*., 2010, 2013].

### 4.3. Relationship Between Spectral and Global Albedo

As noted in equation (3), total upward short-wave solar radiation reflected by ground surface $S_{up}$ can be calculated from ground surface albedo $\alpha_g$ and total downward short-wave radiation $S_{down}$ that reach the ground surface, as shown in the following formula:

$$S_{up} = \alpha_g \times S_{down} \tag{5}$$

The total downward short-wave radiation $S_{down}$ can be divided into the following three spectral wavelength components: UV, VIS, and NIR. Hence, GR can be expressed by a linear combination of spectral radiation, so the equation (5) thus can be rewritten as

$$S_{up} = \alpha_g \times S_{down} = \alpha_{UV} \times S_{UV} + \alpha_{VIS} \times S_{VIS} + \alpha_{NIR} \times S_{NIR} \tag{6}$$

where $S_{UV}$, $S_{VIS}$, and $S_{NIR}$ are UV, VIS, and NIR irradiance and $\alpha_{UV}$, $\alpha_{VIS}$, and $\alpha_{NIR}$ are the ground surface albedo for UV, VIS, and NIR, respectively.

Based on the energy ratios of SR/GR, equation (6) can be rewritten as

$$\begin{aligned} S_{up} &= \alpha_g \times S_{down} \\ &= \alpha_{UV} \times S_{UV} + \alpha_{VIS} \times S_{VIS} + \alpha_{NIR} \times S_{NIR} \\ &= \alpha_{UV} \times f_{UV} \times S_{down} + \alpha_{VIS} \times f_{VIS} \times S_{down} + \alpha_{NIR} \times f_{NIR} \times S_{down} \end{aligned} \tag{7}$$

And then, we can have

$$\alpha_g \times S_{down} = \alpha_{UV} \times f_{UV} \times S_{down} + \alpha_{VIS} \times f_{VIS} \times S_{down} + \alpha_{NIR} \times f_{NIR} \times S_{down} \tag{8}$$

So $\alpha_g$ can be expressed as

$$\alpha_g = \alpha_{UV} \times f_{UV} + \alpha_{VIS} \times f_{VIS} + \alpha_{NIR} \times f_{NIR} \tag{9}$$

where $f_{UV}$, $f_{VIS}$, and $f_{NIR}$ are the energy ratio of UV/GR, VIS/GR, and NIR/GR, respectively. According to equation (9), we can obtain the relationship between SR and GR albedos. GR albedo is determined by the energy ratios of SR/GR and SR albedos.

## 5. Conclusions and Discussion

The objective of this work was to first investigate SR and GR variation features, the energy ratio of SR/GR and corresponding albedo values at typical nonvegetated bare soil underlying surfaces in arid and semiarid and semihumid regions in northwestern China. And then, the observational results are used to be compared with the values prescribed in some LSMs. This comparison validation work can help us to deeply understand, develop, and improve the bare soil albedo parameterization in LSM. Therefore, three field experiments on surface spectral broadband radiation and corresponding albedo were conducted at the three man-made sites over Gobi, desert, and bare loess zones during three different IOP from 2010 to 2013 in Gansu Province northwestern China, respectively. We have gathered the continuous and high temporal resolution records of ground surface radiation, including GR, UV, VIS, and NIR irradiance, and corresponding albedos over three typical nonvegetated underlying surfaces in arid and semiarid and semihumid regions in northwestern China.

The variation trends of the SR (including UV, VIS, and NIR) were coincident with the GR variation at the three sites. The irradiances were gradually decreasing throughout the IOP. The total SR and GR irradiance were significantly affected by synoptic conditions. The identical, regular, and symmetrical distribution shapes is shown in typical sunny days. However, the irregular trends and asymmetrical distribution shapes is shown in cloudy and overcast days. The maximum irradiance values occur at local noon.

For the Gobi, desert, and bare loess land surfaces, the energy ratios of VIS/GR are approximately 40.2%, the ones of NIR/GR are approximately 54.4%. NIR portion is approximately 10%–15% higher than the visible portion. The ratios of VIS/GR and NIR/GR are not 50% as prescribed for all of the soil color classes in most of LSMs.

The averaged surface albedos are 0.231, 0.211, and 0.142 for visible, are 0.266, 0.252, and 0.255 for the NIR over the Gobi, desert, and bare loess land surfaces, respectively. The observational value of the bare soil albedo for NIR is not twice that of the VIS as prescribed for bare soil underlying surfaces in most of LSMs. According to the relationship between SR and GR albedos, we can find that GR albedo is determined by the energy ratios of SR/GR and SR albedos.

The continuous and high-temporal-resolution measurements of SR and GR irradiances may be needed to use for providing the detailed qualitative and quantitative descriptions of the energy ratios of SR/GR and corresponding albedos for typical nonvegetated bare soil underlying surface in northwestern China. It is necessary to investigate the key features of such as the energy ratios of VIS/GR and NIR/GR and soil albedos for VIS and NIR to develop and perfect land surface models. The more field experiments should be planned and carried out in the following years. The data sets collected from the field experiments can be used to further improve and develop LSMs.

**Acknowledgments**

This study was supported by the National Natural Science Foundation of China (grant 41275011 and 41375001) and the Fundamental Research Funds for the Central Universities. The data used in the manuscript, which is supported by the National Natural Science Foundation of China, is not available for proprietary and security reasons. We are very grateful to the Editor and anonymous reviewers for their careful review and valuable comments, which led to substantial improvement of this manuscript.

## References

Ao, Y. H., S. H. Lv, B. Han, and Z. G. Li (2013), Analyses on micrometeorology characteristics in surface layer over Badan Jaran desert in summer [in Chinese with English abstract], *Plateau Meteorol.*, *32*(6), 1683–1691, doi:10.7522/j.issn.1000-0534.2012.00158.

Bai, J. H., Q. X. Kong, and G. R. Liu (1998), Observation and analysis of solar spectral radiation in solar eclipse at Mohe [in Chinese with English abstract], *Acta Energiae Solaris Sin.*, *19*(3), 327–331.

Bala, G., and B. Nag (2012), Albedo enhancement over land to counteract global warming: Impacts on hydrological cycle, *Clim. Dyn.*, *39*(6), 1527–1542, doi:10.1007/s00382-011-1256-1.

Barnes, C. A., and D. P. Roy (2008), Radiative forcing over the conterminous United States due to contemporary land cover land use albedo change, *Geophys. Res. Lett.*, *35*, L09706, doi:10.1029/2008GL033567.

Barnes, C. A., and D. P. Roy (2010), Radiative forcing over the conterminous United States due to contemporary land cover land use change and sensitivity to snow and interannual albedo variability, *J. Geophys. Res.*, *115*, G04033, doi:10.1029/2010JG001428.

Barnett, T. P., et al. (1999), Detection and attribution of recent climate change: A status report, *Bull. Am. Meteorol. Soc.*, *90*, 2631–2659.

Barnett, T. P., et al. (2005), Detecting and attributing external influences on the climate system: A review of recent advances, *J. Clim.*, *18*, 1291–1314.

Bonan, G. B. (1996), A land surface model (LSM version 1.0) for ecological, hydrological, and atmospheric studies: Technical description and user's guide, NCAR Tech. Note NCAR/TN-417 + STR, 29-30 pp.

Bonan, G. B., S. Levis, L. Kergoat, and K. W. Oleson (2002), Landscapes as patches of plant functional types: An integrating concept for climate and ecosystem models, *Global Biogeochem. Cycles*, *16*(2), 1021, doi:10.1029/2000GB001360.

Bsaibes, A., et al. (2009), Albedo and LAI estimates from FORMOSAT-2 data for crop monitoring, *Remote Sens. Environ.*, *113*, 716–729, doi:10.1016/j.rse.2008.11.014.

BurkHardt, U., and B. Karcher (2011), Global radiative forcing from contrail cirrus, *Nat. Clim. Change*, *1*, 54–58, doi:10.1038/NCLIMATE1068.

Charney, J. G. (1975), Dynamics of deserts and drought in the Sahel, *Quart. J. Roy. Meteor. Soc.*, *101*(428), 193–202.

Charney, J., W. J. Quirk, S. H. Chow, and J. Kornfield (1977), A comparative study of the effects of albedo change on drought in semi-arid regions, *J. Atmos. Sci.*, *34*, 1366–1385.

Chen, S. Q., L. J. Wen, S. H. Lv, Y. H. Ao, and Y. Zhang (2006), Analysis of characteristics of radiation on different underlying surface in Jinta oasis [in Chinses with English abstract], *Acta Energige Solaris Sin.*, *27*(7), 713–718, doi:0254-0096(2006)07-0713-06.
Courel, M. F., R. S. Kandel, and S. I. Rasool (1984), Surface albedo and the Sahel drought, *Nature*, *307*(9), 528–531.
Cox, P., and D. Stephenson (2007), Climate change–A changing climate for prediction, *Science*, *317*, 207–208.
Dai, Y. J., et al. (2003), The common land model, *Bull. Am. Meteorol. Soc.*, *84*, 1013–1023, doi:10.1175/BAMS-84-8-1013.
Dickinson, R. E. (1983), Land surface processes and climate surface albedos and energy-balance, *Adv. Geophys.*, *25*, 305–353.
Dickinson, R. E. (1995), Land surface processes in climate models, *Remote Sens. Environ.*, *51*, 27–38.
Dickinson, R. E., and B. Hanson (1984), Vegetation-albedo feedbacks, in *Climate Processes and Climate Sensitivity, Geophys. Monogr*, vol. 29, edited by J. E. Hansen and T. Takshashi, AGU, Washington, D. C.
Dickinson, R. E., A. Henderson-Sellers, and P. J. Kennedy (1993), Biosphere-Atmosphere Transfer Scheme (BATS) Version 1e as coupled to the NACR Community Model, NACR Tech. Note NCAR/TN-387 + STR, 22-23pp.
Ding, Z. W., Z. P. Wen, R. G. Wu, Z. C. Li, J. J. Zhu, W. B. Li, and M. Q. Jian (2013), Surface energy balance measurements of a banana plantation in south China, *Theor. Appl. Climatol.*, *114*, 349–363, doi:10.1007/s00704-013-0849-5.
Dirmeyer, P. A., and J. Shukla (1994), Albedo as a modulator of climate response to tropical deforestation, *J. Geophys. Res.*, *99*, 20,863–20,877, doi:10.1029/94JD01311.
Escobedo, J. F., N. G. Eduardo, P. O. Amauri, and S. Jacyra (2011), Ratios of UV, PAR and NIR components to global solar radiation measured at Botucatu site in Brazil, *Renewable Energy*, *36*, 169–178, doi:10.1016/j.renene.2010.06.018.
Geiger, M., L. M. Diabate, and L. Wald (2002), A web service for controlling the quality of measurements of global radiation, *Sol. Energ.*, *73*, 475–480.
Huber, M., and R. Knutti (2011), Anthropogenic and natural warming inferred from changes in Earth's energy balance, *Nat. Geosci.*, *5*, 31–36, doi:10.1038/ngeo1327.
Iqbal, M. (1983), *An Introduction to Solar Radiation*, vol. XVII, 390 pp., Academic Press Inc., New York.
Ji, F., Z. H. Wu, J. P. Huang, and E. P. Chassignet (2014), Evolution of land surface air temperature trend, *Nat. clim. change-lett.*, *4*, 462–466, doi:10.1038/nclimate2223.
Ji, G. L., X. Y. Ma, J. L. Zou, and L. Z. Lv (1993), Characteristics of the photosynthetically active radiation over Zhangye region [in Chinese with English abstract], *Plateau Meteorol.*, *12*(2), 141–146.
Ji, G. L., X. Y. Ma, J. L. Zou, and L. Z. Lv (2003), Characteristics of the radiation budget over oases in arid region [in Chinese with English abstract], *Arid Meteorol.*, *21*(3), 29–33, doi:1006-7639(2003)-03-0029-05.
Ji, G. L., X. H. Hou, L. Z. Lv, and R. Li (2004), Characteristics of radiation budget on different underlying surfaces in the arid region (in Chinese with English abstract), *Acta Energiae Solaris Sin.*, *25*(1), 37–40, doi:0254-0096(2004)01-0037-04.
Jiang, H. (1993), The spectrum characteristics of global radiation and surface albedo over oasis region in HEIFE [in Chinese with English abstract], *Plateau Meteorol.*, *12*(2), 156–161.
Jin, Y., and D. P. Roy (2005), Fire-induced albedo change and its radiative forcing at the surface in northern Australia, *Geophys. Res. Lett.*, *32*, L13401, doi:10.1029/2005GL022822.
Jones, P. D., M. New, D. E. Parker, S. Martin, and I. G. Rigor (1999), Surface air temperature and its changes over the past 150 years, *Rev. Geophys.*, *37*, 173–199, doi:10.1029/1999RG900002.
Kiehl, J. T., and K. E. Trenberth (1997), Earth's annual global mean energy budget, *Bull. Am. Meteorol. Soc.*, *78*(2), 197–208.
Knutti, R., and G. C. Hegerl (2008), The equilibrium sensitivity of the Earth's temperature to radiation changes, *Nat. Geosci.*, *1*, 735–743, doi:10.1038/ngeo337.
Lawrence, D. M., and A. G. Slater (2008), Incorporating organic soil into a global climate model, *Clim. Dyn.*, *30*, 145–160, doi:10.1007/s00382-007-0278-1.
Lawrence, P. J., and T. N. Chase (2007), Representing a MODIS consistent land surface in the Community Land Model (CLM 3.0), *J. Geophys. Res.*, *112*, G01023, doi:10.1029/2006JG000168.
Li, Z. C., Z. G. Wei, J. Wen, T. T. Zhang, and Y. Y. Liu (2008), Study of land surface radiation and energy balance at winter wheat fields over typical mesa of Chinese Loess Plateau [in Chinese with English abstract], *Clim. Environ. Res.*, *13*(6), 751–758, doi:1006-9585(2008)06-0751-08.
Li, Z. C., Z. G. Wei, J. Wen, R. Fu, Y. Y. Liu, and R. Liu (2009), Analysis of land-surface radiation characteristic in winter-wheat field over the Loess Plateau mesa in China [in Chinese with English abstract], *Acta Energige Solaris Sin.*, *30*(1), 12–18, doi:0254-0096(2009)01-0012-07.
Liang, S. L., K. C. Wang, X. T. Zhang, and M. Wild (2010), Review on estimation of land surface radiation and energy budgets from ground measurement, remote sensing model simulations, *IEEE J. Special Topics Appl. Earth Obs. Remote Sens.*, *3*(3), 225–240, doi:10.1109/JSTARS.2010.2048556.
Liang, S. L., et al. (2013), A long-term Global LAnd Surface Satellite (GLASS) data-set for environmental studies, *Int. J. Digital Earth*, *6*(1), 34–49, doi:10.1080/17538947.2013.805262.
Liu, N. F., Q. Liu, L. Z. Wang, S. L. Liang, J. G. Wen, Y. Qu, and S. H. Liu (2013), A statistics-based temporal filter algorithm to map spatiotemporally continuous shortwave albedo from MODIS data, *Hydrol. Earth Syst. Sci.*, *17*, 2121–2129, doi:10.5194/hess-17-2121-2013.
Liu, Q., L. Z. Wang, Y. Qu, N. F. Liu, S. H. Liu, H. R. Tang, and S. L. Liang (2013), Preliminary evaluation of the long-term GLASS albedo product, *Int. J. Digital Earth*, *6*(1), 34–49, doi:10.1080/17538947.2013.804601.
Loew, A., and Y. Govaerts (2010), Towards multidecadal consistent Meteosat surface albedo time series, *Remote Sens.*, *2*, 957–967, doi:10.3390/rs2040957.
Manalo-Smith, N., G. L. Smith, S. N. Tiwari, and W. F. Staylor (1998), Analytic forms of bidirectional reflectance functions for application to Earth radiation budget studies, *J. Geophys. Res.*, *103*, 19,733–19,751, doi:10.1029/98JD00279.
Meng, X. H., J. P. Evans, and M. F. McCabe (2013), The influence of inter-annually varying albedo on regional climate and drouht, *Clim. Dyn.*, *42*, 787–803, doi:10.1007/s00382-013-1790-0.
Mercado, L. M., N. Bellouin, S. Sitch, O. Boucher, C. Huntingford, M. Wild, and P. M. Cox (2009), Impact of changes in diffuse radiation on the global land carbon sink, *Nat. Lett.*, *458*, 1014–1018, doi:10.1038/nature07949.
Moritz, R. E., C. M. Bitz, and E. J. Steig (2002), Dynamics of recent climate change in the arctic, *Science*, *297*, 1497–1502, doi:10.1126/science.1076522.
Murphy, D. M., S. Solomon, R. W. Portmann, K. H. Rosenlof, P. M. Forster, and T. Wong (2009), An observationally based energy balance for the Earth since 1950, *J. Geophys. Res.*, *114*, D17107, doi:10.1029/2009JD012105.
Nicolaus, M., S. Gerland, S. R. Hudson, S. Hanson, J. Haapala, and D. K. Perovich (2010), Seasonality of spectral albedo and transmittance as observed in the Arctic Transpolar Drift in 2007, *J. Geophys. Res.*, *115*, C11011, doi:10.1029/2009JC006074.
Nikitidou, E., and A. Kazantzidis (2013), On the differences of ultraviolet and visible irradiance calculations in the Mediterranean basin due to model- and satellite-derived climatologies of aerosol optical properties, *Int. J. Climatol.*, *33*, 2877–2888, doi:10.1002/joc.3638.

Oleson, K. W., et al. (2010), Technical description of version 4.0 of the Community Land Model (CLM), NACR/TN-503+STR/NACR Tech. Note, 36–38 pp.
Oleson, K. W., et al. (2013), Technical description of version 4.5 of the Community Land Model (CLM), NACR/TN-487+STR/NACR Tech. Note, 46–48 pp.
Overpeck, J. T., G. A. Meechl, S. Bony, and D. R. Easterling (2011), Climate data challenges in the 21st century, *Science*, *331*, 700, doi:10.1126/science.1197869.
Qu, Y., Q. Liu, S. L. Liang, L. Wang, N. F. Liu, and S. H. Liu (2013), Direct-estimation algorithm for mapping daily land-surface broadband albedo from MODIS data, *IEEE Trans. Geosci. Remote Sens.*, 1–13, doi:10.1109/TGRS.2013.2245670.
Rigby, M., et al. (2014), Recent and future trends in synthetic greenhouse gas radiative forcing, *Geophys. Res. Lett.*, *41*, 2623–2630, doi:10.1002/2013GL059099.
Sellers, P. J., Y. Mintz, Y. C. Sud, and A. Dalcher (1986), A simple biosphere model (SiB) for use within general circulation models, *J. Atmos. Sci.*, *43*, 505–531.
Shi, G. Y., T. Hayasaka, A. Ohmura, Z. H. Chen, B. Wang, J. Q. Zhao, H. Z. Che, and L. Xu (2008), Data quality assessment and the long-term trend of ground solar radiation in China, *J. Appl. Meteorol. Climatol.*, *17*, 1006–1016, doi:10.1175/2007JAMC1493.1.
Soloman, S., et al. (2007), *IPCC Climate Change 2007: The Physical Science Basis*, 996 pp., Cambridge Univ. Press, Cambridge, U. K., and New York.
Stocker, T. F., et al. (2013), *IPCC Climate Change 2013: The Physical Science Basis*, 1535 pp., Cambridge Univ. Press, Cambridge, U. K., and New York, doi:10.1017/CB09781107415324.
Tett, S. F. B., P. A. Stott, M. R. Allen, W. J. Ingram, and J. F. B. Mitchell (1999), Causes of twentieth-century temperature change near the Earth's surface, *Nature*, *399*, 569–572.
Thies, B., and J. Bendix (2011), Satellite based remote sensing of weather and climate: Recent achievements and future perspectives, *Meteorol. Appl.*, *18*, 262–295, doi:10.1002/met.288.
Trenberth, K. E., and J. T. Fasullo (2009), Global warming due to increasing absorbed solar radiation, *Geophys. Res. Lett.*, *36*, L07706, doi:10.1029/2009GL037527.
Trenberth, K. E., et al. (2007), Observations: Surface and atmospheric climate change, in *Climate Change 2007: The Physical Science Basis. Contribution of Working Group I to the Fourth Assessment Report of the Intergovernmental Panel on Climate Change*, edited by S. Solomon et al., pp. 236–247, Cambridge Univ. Press, Cambridge, U. K., and New York.
Trenberth, K. E., J. T. Fasullo, and J. Kiehl (2008), Earth's global energy budget, *Bull. Am. Meteorol. Soc.*, *90*, 311–323, doi:10.1175/2008BAMS2634.1.
Tsvetsinskaya, E. A., C. B. Schaaf, F. Gao, A. H. Strahler, R. E. Dickinson, X. Zeng, and W. Lucht (2002), Relating MODIS-derived surface albedo to soil and rock types over Northern Africa and the Arabian Peninsula, *Geophy. Res. Lett.*, *29*, 1353, doi:10.1029/2001GL014096.
Wang, C., Z. G. Wei, Z. C. Li, H. Liu, and H. Wei (2012), Study on variation of net radiation in the dunhuang gobi [in Chinese with English abstract], *Arid Zone Res.*, *29*(2), 251–256.
Wang, K. C. (2014), Sampling biases in datasets of historical mean air temperature over land, *Sci. Rep.*, *4*, 4637, doi:10.1038/srep04637.
Wang, K. C., and R. E. Dickinson (2013), Contribution of solar radiation to decadal temperature variability over land, *Proc. Natl. Acad. Sci. U.S.A.*, doi:10.1073/pnas.1311433110.
Wang, K. C., R. E. Dickinson, Q. Ma, J. A. Augustine, and M. Wild (2013), Measurement methods affect the observed global dimming and brightening, *J. Clim.*, *26*, 4112–4120, doi:10.1175/JCLI-D-12-00482.1.
Wang, S., R. F. Grant, D. L. Verseghy, and T. A. Black (2001), Modelling plant carbon and nitrogen dynamics of a boreal aspen forest in CLASS-the Canadian Land surface Scheme, *Ecol. Model.*, *142*(1–2), 135–142.
Wang, S., R. F. Grant, D. L. Verseghy, and T. A. Black (2002a), Modelling carbon dynamics of a boreal forest in ecosystems using the Canadian Land surface Scheme, *Clim. Change.*, *55*(4), 451–477.
Wang, S., R. F. Grant, D. L. Verseghy, and T. A. Black (2002b), Modelling carbon-coupled energy and water dynamics of a boreal aspen forest in general circulation model Land surface Scheme, *Int. J. Climatol.*, *22*, 1249–1265, doi:10.1002/joc.776.
Wang, S., Q. Zhang, and G. A. Wei (2004), Simulation of land-surface characteristic under precipitation condition in Dunhuang Arid Region [in Chinese with English abstract], *Arid Meteorol.*, *22*(4), 46–50.
Wang, S., Q. Zhang, and G. A. Wei (2005), Analyses on characters of surface radiation and energy at oasis-desert transition zone in Dunhuang [in Chinese with English abstract], *Plateau Meteorol.*, *24*(4), 556–562, doi:1000-0534(2005)04-0556-07.
Wang, S., Q. Zhang, and H. Zhang (2008), Characteristics of surface albedo and soil heat conductivity in spare vegetation site [in Chinese with English abstract], *J. Desert Res.*, *28*(1), 119–124, doi:1000-694X(2008)01-0119-06.
Wang, Z., X. Zeng, M. Barlage, R. E. Dickinson, F. Gao, and C. B. Schaaf (2004), Using MODIS BRDF and albedo data to evaluate global model land surface albedo, *J. Hydrometeorol.*, *5*, 1–14.
Wei, X., A. N. Hahamann, R. E. Dickinson, Z.-L. Yang, X. B. Zeng, K. J. Schaudt, C. B. Schaaf, and N. Strugnell (2001), Comparison of albedos computed by land surface models and evaluation against remotely sensed data, *J. Geophys. Res.*, *106*, 687–702, doi:10.1029/2001JD900218.
Wei, Y. H., and Z. Y. Lin (1992), Geographic distribution characteristics of the solar spectral radiation in the west Kunlun Mountain region [in Chinese with English abstract], *Plateau Meteorol.*, *11*(3), 249–258.
Wei, Z. G., J. Wen, S. H. Lv, S. Q. Chen, Y. H. Ao, and L. Liang (2005), A primary filed experiment of land-atmosphere interaction over the Loess Plateau and its ground surface energy in clear days [in Chinese with English abstract], *Plateau Meteorol.*, *24*(4), 545–555.
Wei, Z. G., R. H. Huang, and W. Chen (2006), Transfer coefficients of sensible heat under the atmospheric stability in near surface layer over Dunhuang Gobi [in Chinese with English abstract], *Plateau Meteorol.*, *25*(2), 834–839, doi:1000-0534(2006)05-0834-06.
Wielicki, B. A., T. Wong, N. Loeb, P. Minnis, K. Priestley, and R. Kandel (2005), Changes in Earth's albedo measured by satellite, *Science*, *308*(5723), 825.
Wilson, M. F., A. Henderson-Sellers, R. E. Dickinson, and P. J. Kenney (1987), Sensitivity of Biosphere-Atmosphere Transfer Scheme (BATS) to the inclusion of variable soil characteristics, *J. Clim. Appl. Meteorol.*, 341–362.
Xiong, X. Z., X. Y. Wang, G. C. Wang, S. K. Zhang, H. B. Yu, and X. S. Liu (1994), Characteristics of solar spectral radiation in the Guangzhou district [in Chinese with English abstract], *Q. J. Appl. Meteorol.*, *5*(1), 98–103.
Xue, Y., and A. P. Cracknell (1995), Operational bi-angle approach to retrieve the Earth surface albedo from AVHRR data in the visible band, *Int. J. Remote. Sensing*, *16*(3), 417–429.
Xue, Y., P. J. Sellers, J. L. Kinter, and J. Shukla (1991), A simplified biosphere model for global climate studies, *J. Clim.*, *4*, 345–364.
Xue, Y., F. J. Zeng, and C. A. Schlosser (1996), SSiB and its sensitivity to soil properties a case study using HAPEX-Mobilhy data, *Global Planet. Change*, *13*, 183–194.

Yang, J., P. Gong, R. Fu, M. H. Zhang, J. M. Chen, S. L. Liang, B. Xu, J. C. Shi, and R. Dickinson (2013), The role of satellite remote sensing in climate change studies, *Nat. Clim. Change*, *3*, 875–883, doi:10.1038/nclimate1908.

Yang, X. G., P. L. Ma, R. Y. Wang, Q. G. Yang, and H. Y. Liu (2005), Summer land-surface radiation characteristic over Longzhong Region of Loess Plateau, China [in Chinese with English abstract], *J. Desert Res.*, *25*(1), 55–62, doi:1000-694X(2005)01-0055-08.

Zhang, Q., and Y. Zhou (2002), The characteristics of budget of radiation and energy as well microclimate of Dunhuang oasis on a typical clear day in summer [in Chinese with English abstract], *Acta Phytoecol. Sin.*, *26*(6), 717–723.

Zhang, T. T., J. Wen, Z. B. Su, D. R. Veelde, J. Timmermans, R. Liu, Y. Y. Liu, and Z. C. Li (2009), Soil moisture mapping over the Chinese Loess Plateau using the ENVISAT/ASAT data, *Adv. Space Res.*, *43*(7), 1111–1117, doi:10.1016/j.asr.2008.10.030.

Zhang, T. T., J. Wen, Z. G. Wei, R. van der Velde, Z. C. Li, R. Liu, S. N. Lv, and H. Chen (2014), Land-atmospheric water and energy cycle of winter wheat, Loess Plateau, China, *Int. J. Climatol.*, *34*, 3044–3053, doi:10.1002/joc.3891.

Zhang, X. Z., Q. D. Wang, and Y. G. Zhang (1996), The spectral measurement of the solar global radiation on Tibetan Plateau during April-October [in Chinese with English abstract], *Acta Meteorol. Sin.*, *54*(5), 620–624.

Zheng, Z. Y., Z. G. Wei, Z. C. Li, and C. Wang (2012), Characteristics of solar spectral radiation and albedo during early autumn in Dunhuang Gobi [in Chinese with English abstract], *Acta Energiae Solaris Sin.*, *33*(11), 1937–1943, doi:0254-0096(2012)11-1937-07.